Electronic Supplementary Material (ESI) for Physical Chemistry Chemical Physics.

Drying-induced Atomic Structural Rearrangements in Sodium-based Calcium-alumino-silicate-hydrate Gel and the Mitigating Effects of ZrO_2 Nanoparticles

Kengran Yang[1], V. Ongun Özçelik[1], Nishant Garg[1], Kai Gong[1] and Claire E. White[1]*

[1]Department of Civil & Environmental Engineering and Andlinger Center for Energy and the Environment, Princeton University, Princeton, USA

* Corresponding author: Phone: +1 609 258 6263, Fax: +1 609 258 2799, Email: whitece@princeton.edu

Electronic Supplementary Information (ESI)

Local atomic structural changes during formation of silicate-activated slag with and without nano-ZrO_2

The pair distribution function (PDF) data for the control silicate-activated slag sample at different stages during the alkali-activation reaction are shown in Figure S1a. Peak assignments have been carried out based on the investigations by Meral *et al*.,[1] Skinner *et al*.,[2] and Gong and White.[3] Also given in Figure S1a are the difference plots obtained by subtracting the PDF at 24 hrs from the PDF data at different times (the lower subplot in Figure S1a). It is apparent in Figure S1a that the T-O peak at ~ 1.65 Å (T denotes tetrahedral Si or Al) measured at 3600 hrs (~ 150 days) is different from the data measured within the first few days after mixing. This is likely due to the slightly different experimental setups for the two measurements. The peak at ~ 2.0 Å is attributed to the Al/Mg-O correlation in the hydrotalcite-like phase formed in the silicate-activated slag paste,[3] where the intensity is seen to increase over time, indicating continual growth of the aluminum/magnesium oxide sheet associated with hydrotalcite.

The nearest-neighbor and next nearest-neighbor Ca-O correlations at 2.35 Å and 4.52 Å are seen to increase in intensity with time, indicating ongoing formation of C-(N)-A-S-H gel. The significant increase of the Ca-T peak intensity at 3.65 Å is another strong indicator of the continual formation of C-(N)-A-S-H gel, since this peak represents the atomic distance between the calcium atoms in the calcium oxide sheet or in the interlayer spacing and the Si/Al atoms in the aluminosilicate chains of the tobermorite-like C-(N)-A-S-H gel structure. Besides the change in intensity of these peaks, the width of Si-T peak at ~ 3.1 Å decreases with time, indicating that the local bonding environment around the silicon atoms is becoming more ordered, possibly due to

the alumina/silica in slag being transformed into a more ordered chain-like structure in the C-(N)-A-S-H gel.

The evolution of the PDF data for the control silicate-activated slag sample shown here is similar to previous data reported in earlier studies focusing on the kinetics of the alkali-activation reaction.[4,5] Furthermore, the PDF data for the control silicate-activated slag sample containing nano-ZrO_2 (Figure S1b) are qualitatively similar to the PDF data without nano-ZrO_2, revealing that the addition of nano-ZrO_2 (at low concentrations, 0.167% wt. relative to anhydrous slag) does not impact the atomic structure of the C-(N)-A-S-H gel that precipitates in silicate-activated slag during the alkali-activation reaction. However, as discussed later in the ESI, nano-ZrO_2 does appear to slightly affect the kinetics of growth of the C-(N)-A-S-H gel.

(a)

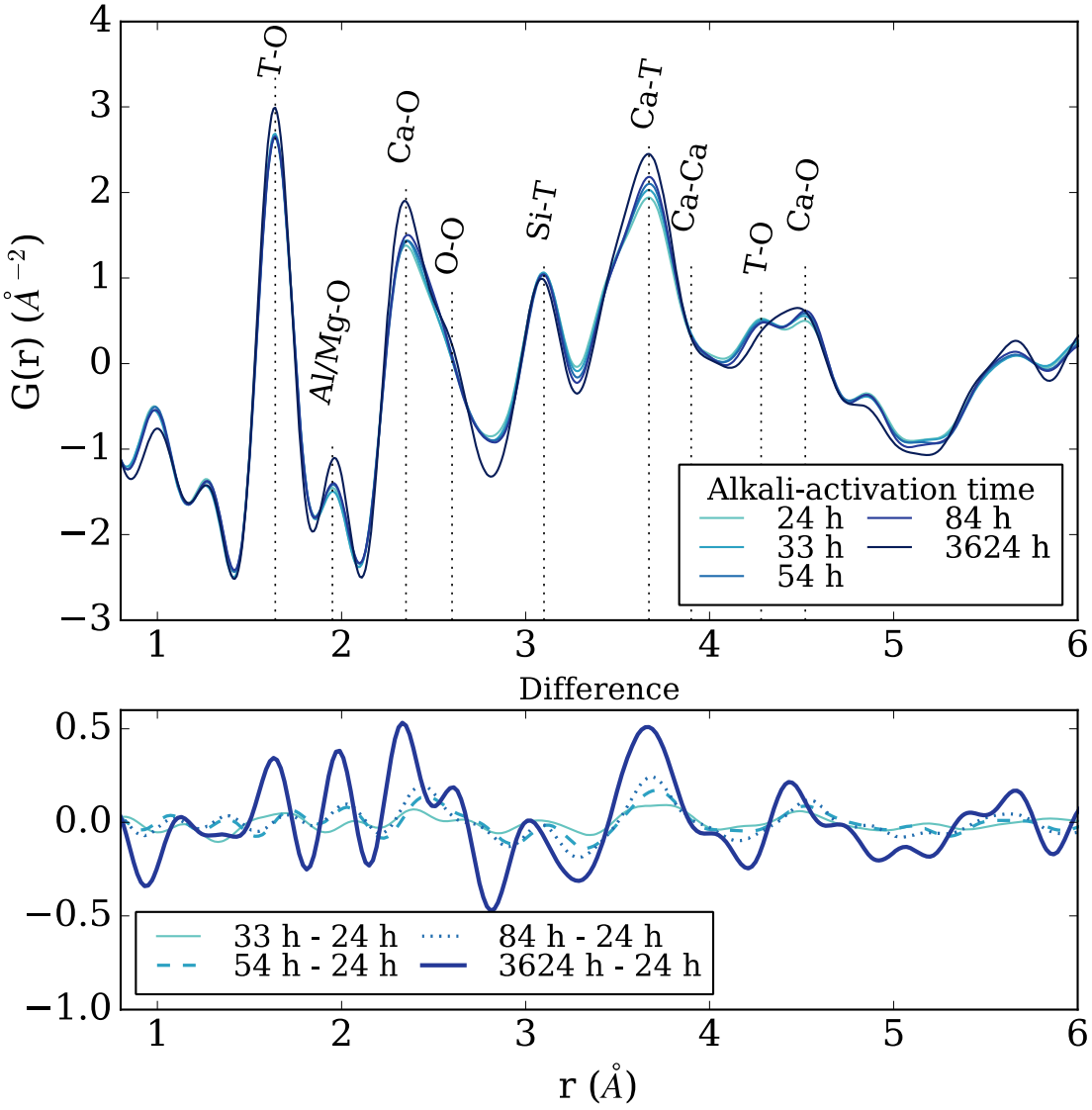
T-O
Al/Mg-O
Ca-O
O-O
Si-T
Ca-T
Ca-Ca
T-O
Ca-O
G(r) (Å^{-2})
Alkali-activation time
24 h
33 h
54 h
84 h
3624 h
Difference
33 h - 24 h
54 h - 24 h
84 h - 24 h
3624 h - 24 h
r (Å)

(b)

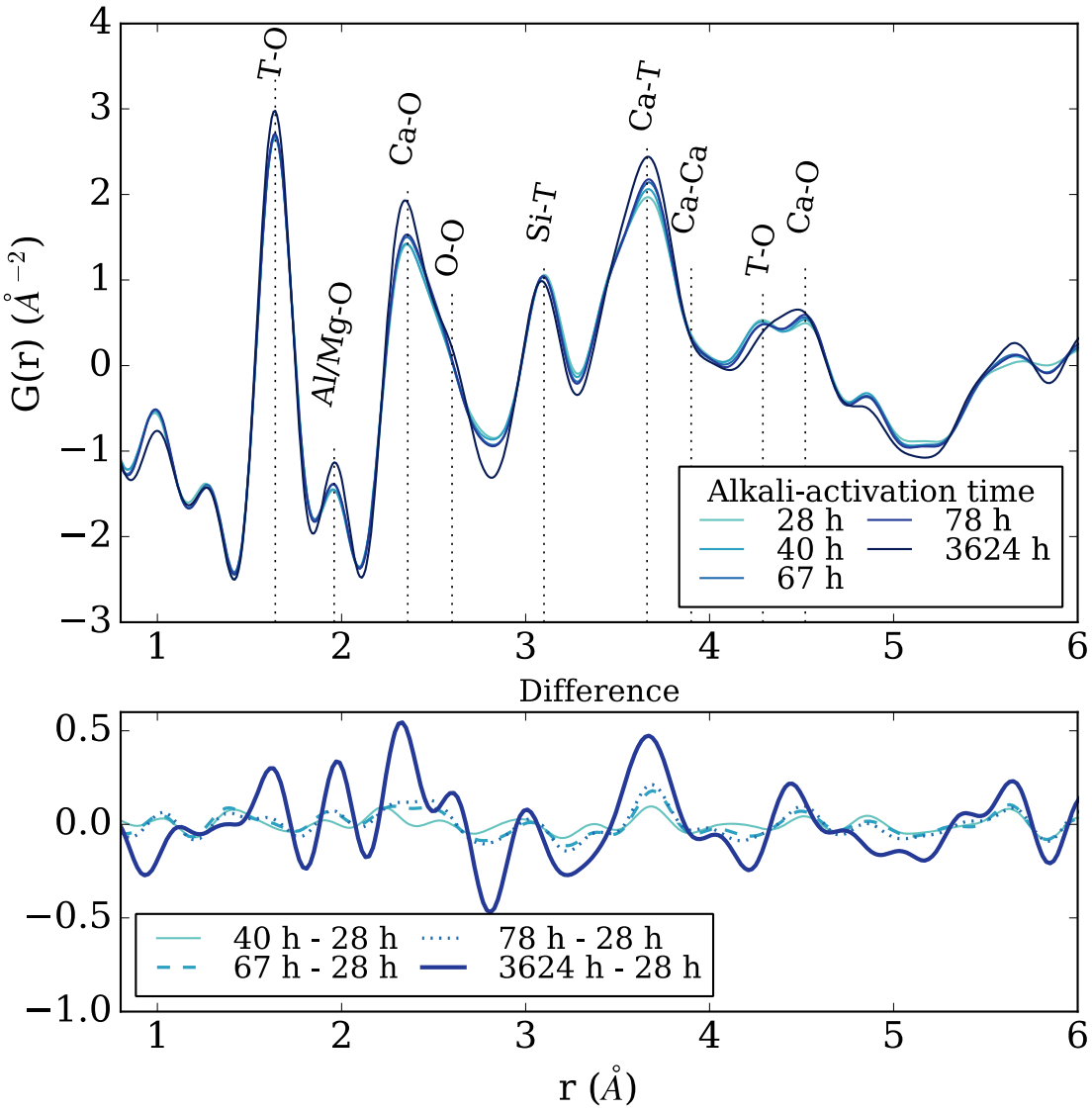

Figure S1. Synchrotron X-ray PDF curves of the alkali-activation reaction for silicate-activated slag (a) without, and (b) with nano-ZrO_2. PDF curves at different alkali-activation times (top), and difference curves of the PDF data obtained via subtraction of the PDF data set acquired 24/28 hrs after mixing (bottom).

Local atomic structural changes of silicate-activated slag with and without nano-ZrO_2 subjected to 43% relative humidity

Figure S2 shows the evolution of the PDF data for silicate-activated slag with and without nano-ZrO_2 in the 43% relative humidity (RH) environment. It can be observed in Figure S2a that the changes invoked in silicate-activated slag when exposed to a moderate drying environment are minimal, as are reflected in the difference plot. This is due to the removal of water only from the gel (and capillary) pores, causing contraction of the paste but not disintegration of the C-(N)-A-S-H gel, which will only happen when interlayer water evaporates.[6] Although some contraction of the silicate-activated slag paste occurs at this RH (see main article for details) there are limited changes seen in the atomic structure (Figure S2a).

On the other hand, significant atomic changes occur in the silicate-activated slag with nano-ZrO_2 in the 43% RH environment (Figure S2b), where the changes are similar to those seen for the silicate-activated slag with nano-ZrO_2 in the 0% RH environment (Figure 6 in the main article). The increase in the Ca-O (first and second nearest-neighbor) and Ca-T peak intensities indicate growth of the "unconventional" gel. Moreover, the increase in the Si-T peak suggests that the silicate species in the paste have a higher degree of polymerization compared with those that are involved in the alkali-activation reaction (since the Si-T intensity in the PDF of the control silicate-activated slag with nano-ZrO_2 is relatively stable throughout the measurement time (Figure S1b)).

(a)

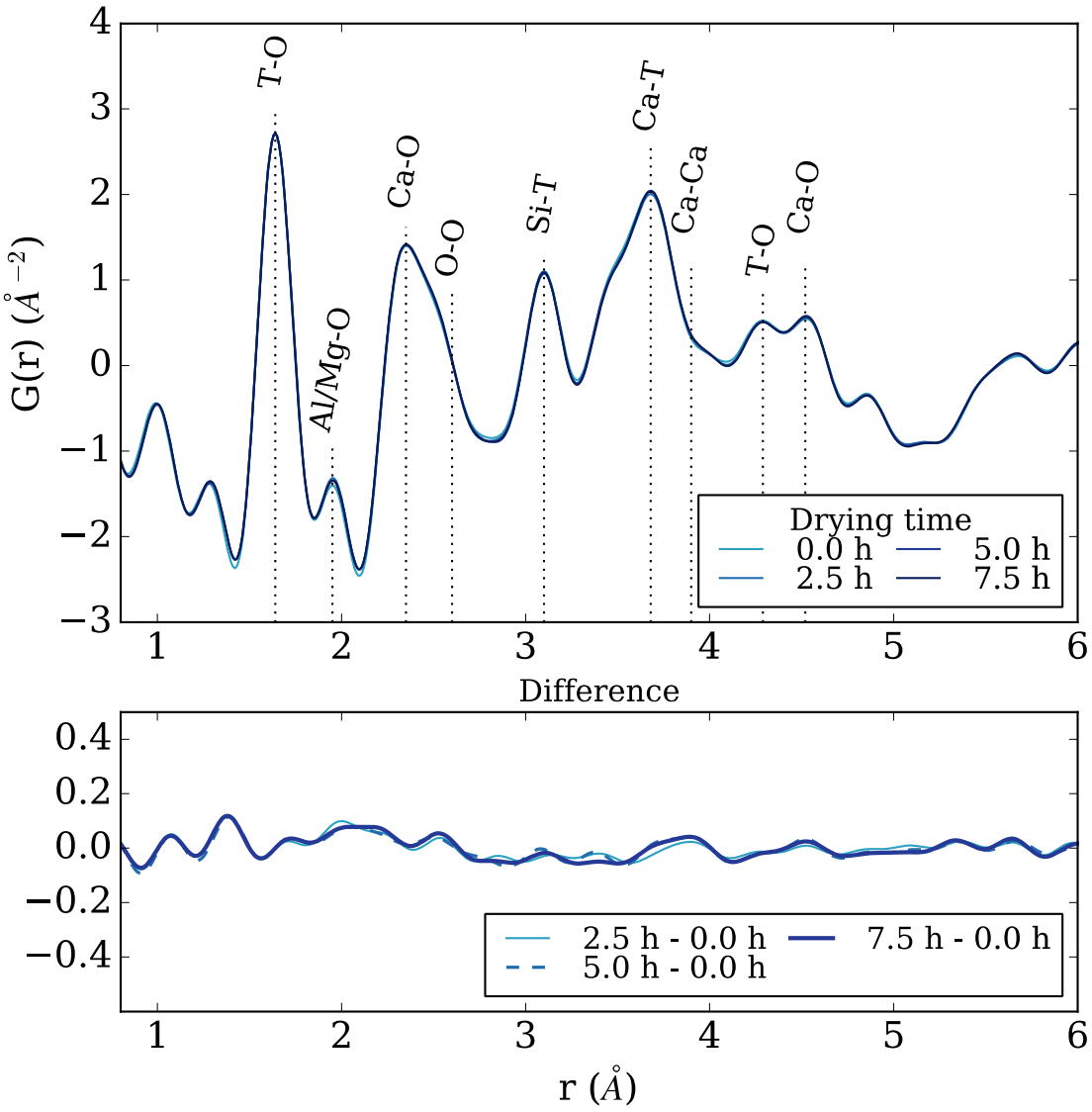
T-O
Al/Mg-O
Ca-O
O-O
Si-T
Ca-T
Ca-Ca
T-O
Ca-O
G(r) (Å^{-2})
Drying time
0.0 h
2.5 h
5.0 h
7.5 h
Difference
2.5 h - 0.0 h
5.0 h - 0.0 h
7.5 h - 0.0 h
r (Å)

(b)

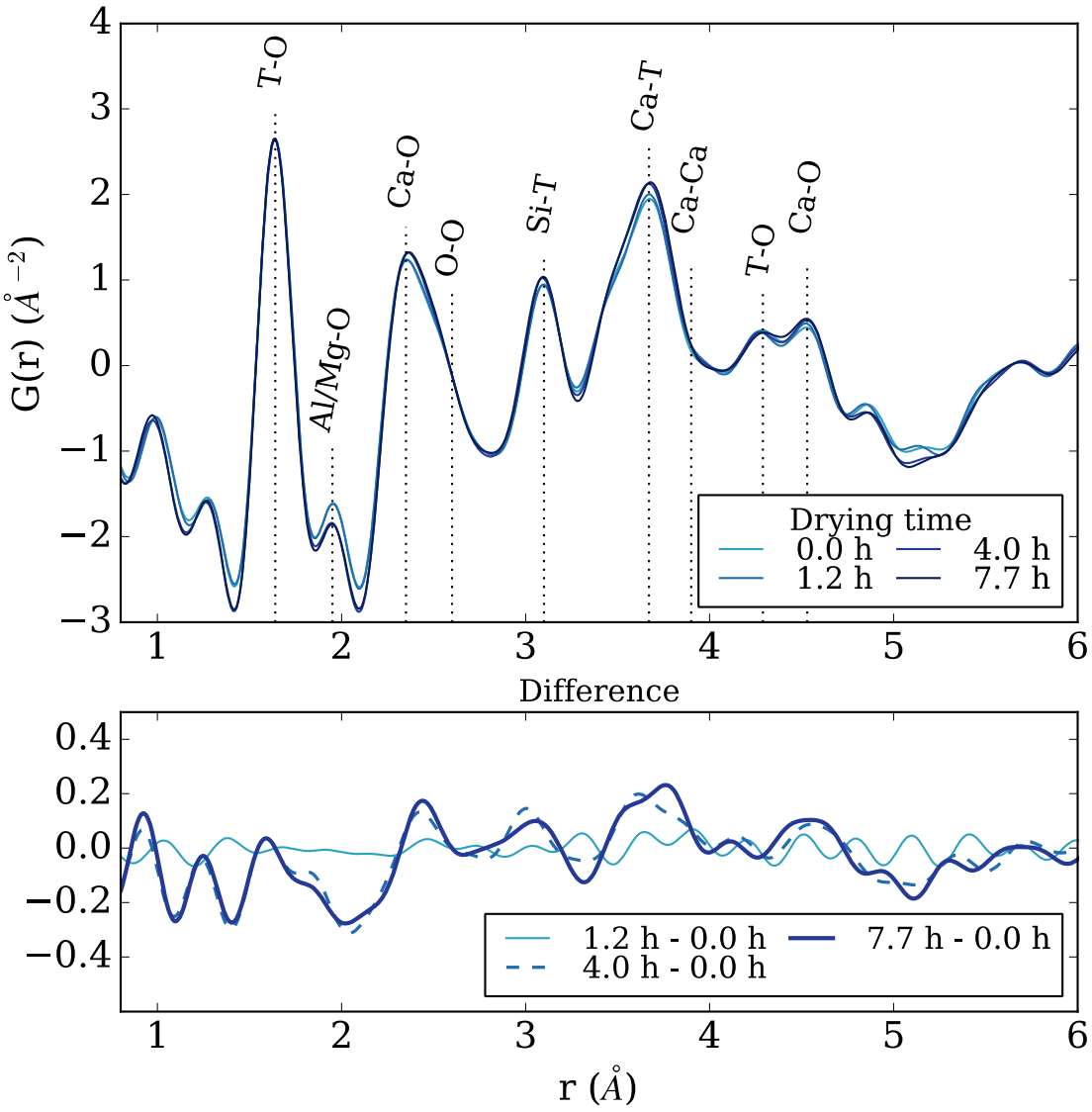

Figure S2. Synchrotron X-ray PDF curves of silicate-activated slag (a) without, and (b) with nano-ZrO_2 subjected to 43% RH. PDF curves at different drying times (top), and difference curves of the PDF data obtained via subtraction of the initial PDF data set (bottom).

Do the atom-atom correlations from liquid water account for the PDF changes seen at 0% RH?

To ensure that the trend shown in Figure 1a in the main article is not only due to the removal of water molecules, but also to the changes in the C-(N)-A-S-H gel structure, the difference plots showing the relative changes from the initial PDF curve (0 hr) to those at longer times are examined. Neutron PDF curves of liquid water at $25°C$ show that intermolecular O-H, H-H and O-O peaks occur at 1.86, 2.29 and 2.85 Å, respectively.[7] A review of the X-ray PDF data for liquid water also shows the presence of the intermolecular O-O peak at 2.80(1) Å, even though hydrogen-related peaks are less visible due to the small X-ray scattering strength of the hydrogen atom.[8] Thus, if the changes in the PDF curves in Figure 1a are solely due to the removal of water molecules, we should observe a decrease in intensity at these peak locations in the difference plot. However, the difference plot shows that there is an increase in intensity at ~ 1.8 Å, and minimal change at ~ 2.3 and 2.8 Å. The drop of intensity at ~ 2.6 Å, however, is probably due to the loss of chemically bonded water, which may have different intermolecular distances compared to bulk water. On the other hand, as water is removed from the sample due to drying, it is expected that the sloping baseline visible in the data at low r values (below ~ 1.5 Å), which is directly related to the atomic number density of the sample, will become shallower with time as seen in Figure 1a and S2a.

X-ray diffraction data of the silicate-activated slag samples during alkali-activation

The X-ray diffraction data of the silicate-activated slag samples with and without nano-ZrO_2 undergoing the alkali-activation reaction are shown in Figure S3. Two major phases are identified: calcium-silicate-hydrate (C-S-H) (denoted as "C", PDF # 00-034-0002), which has a similar

atomic structure to the C-(N)-A-S-H gel, and hydrotalcite (denoted as "H", PDF # 00-014-0191).[5] It is clearly seen in Figure S3a that the Bragg peak intensities of both the C-(N)-A-S-H and hydrotalcite-like phases in silicate-activated slag without nanoparticles increase over time, indicating continual growth of the major reaction products as the alkali-activation reaction progresses. The peak at ~ 0.42 $Å^{-1}$, which represents the interlayer spacing of the C-(N)-A-S-H gel, does not show a systematic trend, likely because of overlap with the beam stop. Comparing Figure S3a with S3b reveals that the addition of nano-ZrO_2 does not have a significant impact on the growth of the main reaction products during the alkali-activation reaction.

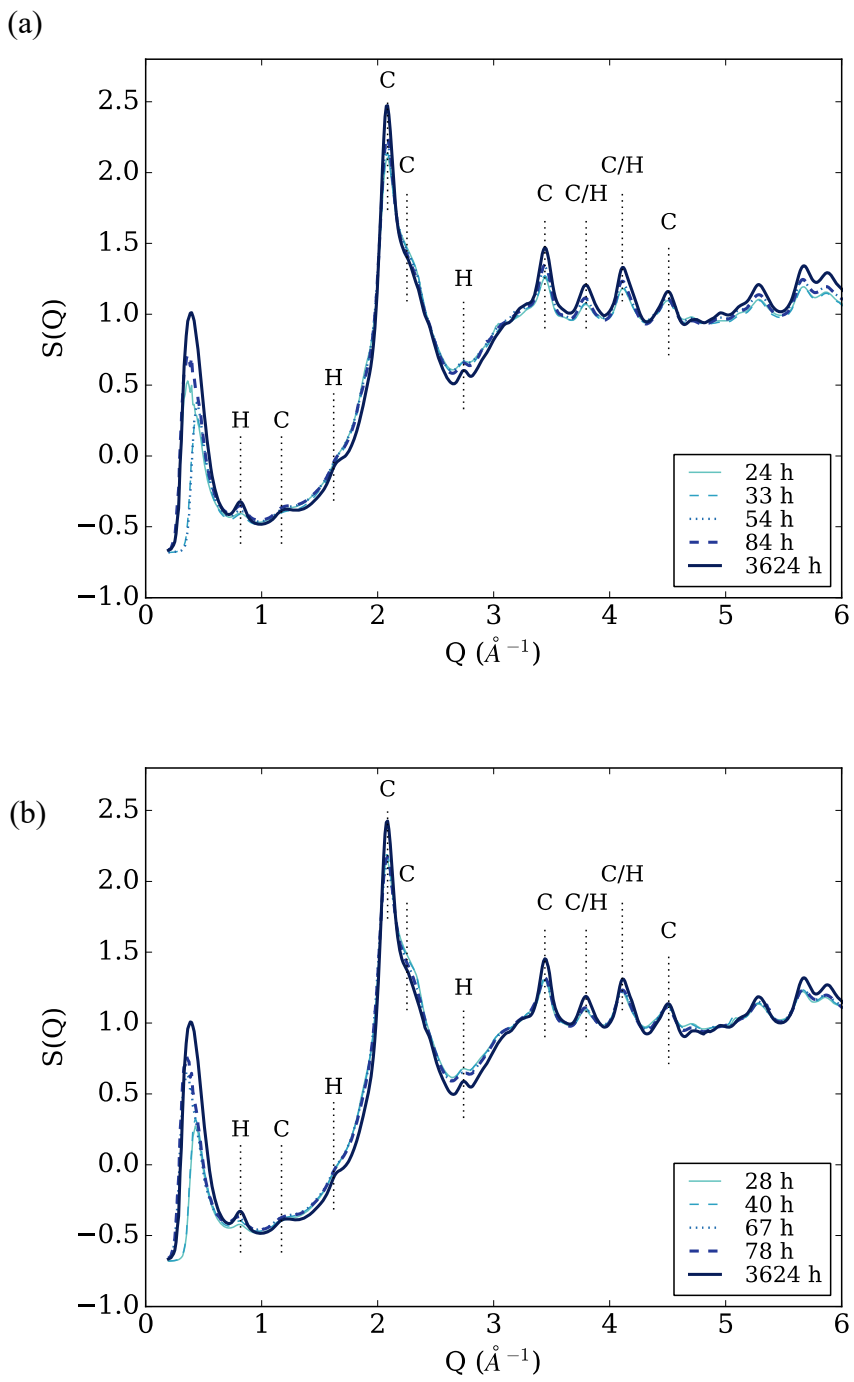

Figure S3. X-ray diffraction patterns of the control silicate-activated slag sample (a) without and (b) with nano-ZrO_2 as a function of alkali-activation time. “C” denotes C-(N)-A-S-H phase while “H” represents the hydrotalcite-like phase.

X-ray diffraction data of silicate-activated slag with and without nano-ZrO_2 subjected to drying

The X-ray diffraction data of silicate-activated slag with and without nano-ZrO_2 subjected to 0% and 43% RH are shown in Figure S4 and S5, respectively. The insets in these figures contain zoomed-in portions of the peak representing the C-(N)-A-S-H gel basal spacing. It is seen that no other crystalline phases emerge during drying of silicate-activated slag (with or without nano-ZrO_2). The inset in Figure S4a clearly shows a shift of the peak at ~ 0.42 $Å^{-1}$ to higher Q spacing for silicate-activated slag without nano-ZrO_2 during drying at 0% RH, indicating a decrease of the C-(N)-A-S-H gel interlayer spacing. This basal spacing corresponds to an interlayer distance of ~14 Å in real space, and the extent of the shift is ~ 0.6 Å, calculated by the relationship $Q = \frac{2\pi}{d}$. On the other hand, the changes seen in the diffraction data for silicate-activated slag with nano-ZrO_2 exposed to 0% RH are less apparent. Figure S4b shows a slight increase in the intensity of the peak denoting the C-(N)-A-S-H gel basal spacing, but this peak does not shift in Q space. The increase in intensity points toward potential growth of the C-(N)-A-S-H gel, however, there are no significant changes visible in the other peaks associated with the gel. Contrary to the changes seen in the diffraction data for silicate-activated slag (with and without nano-ZrO_2) at 0% RH, the diffraction data for silicate-activated slag at 43% RH do not show any evident changes as a result of drying (see Figure S5).

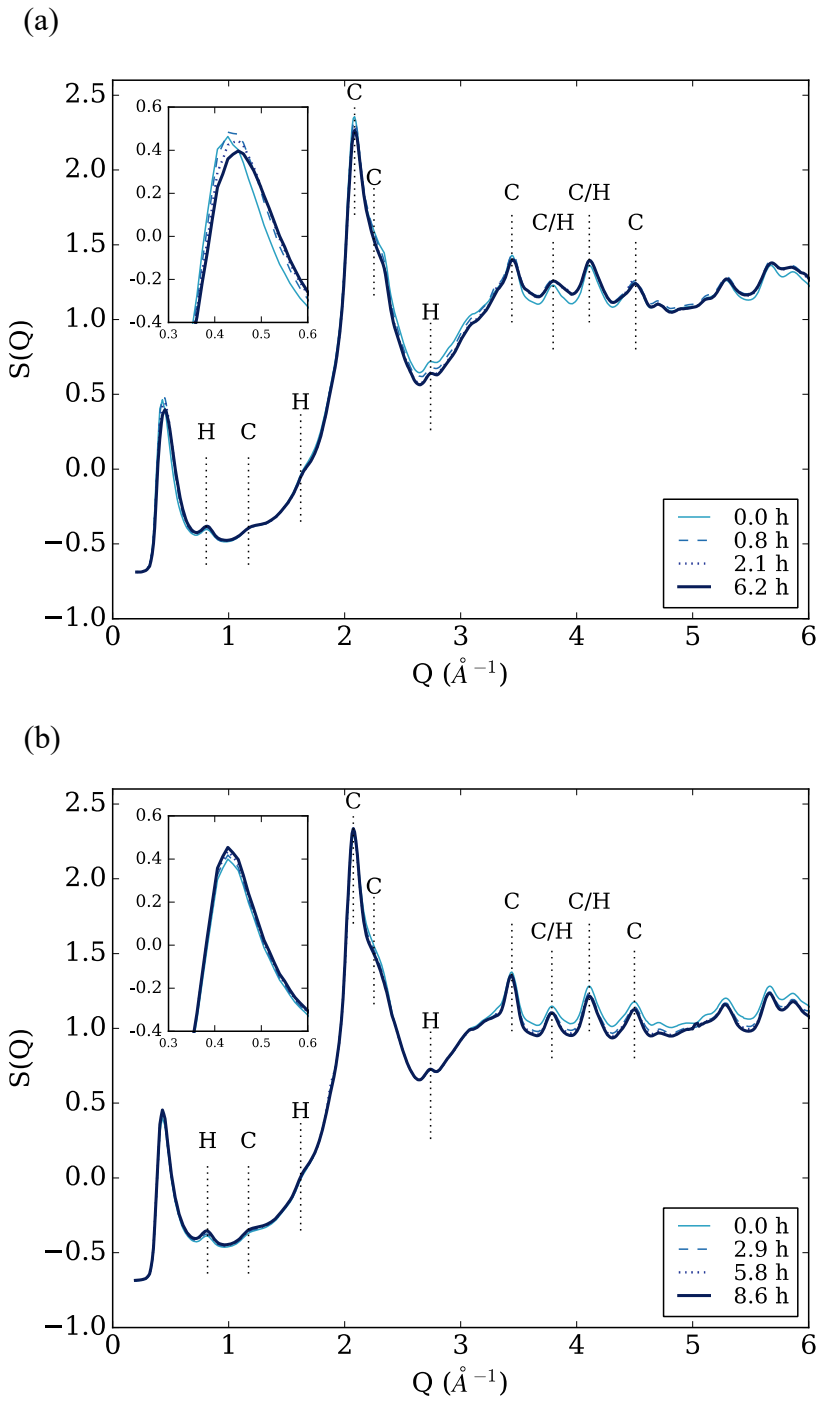

Figure S4. X-ray diffraction patterns of the silicate-activated slag sample (a) without and (b) with nano-ZrO_2 in 0% RH environment as a function of time. "C" denotes the C-(N)-A-S-H phase while "H" represents the hydrotalcite-like phase.

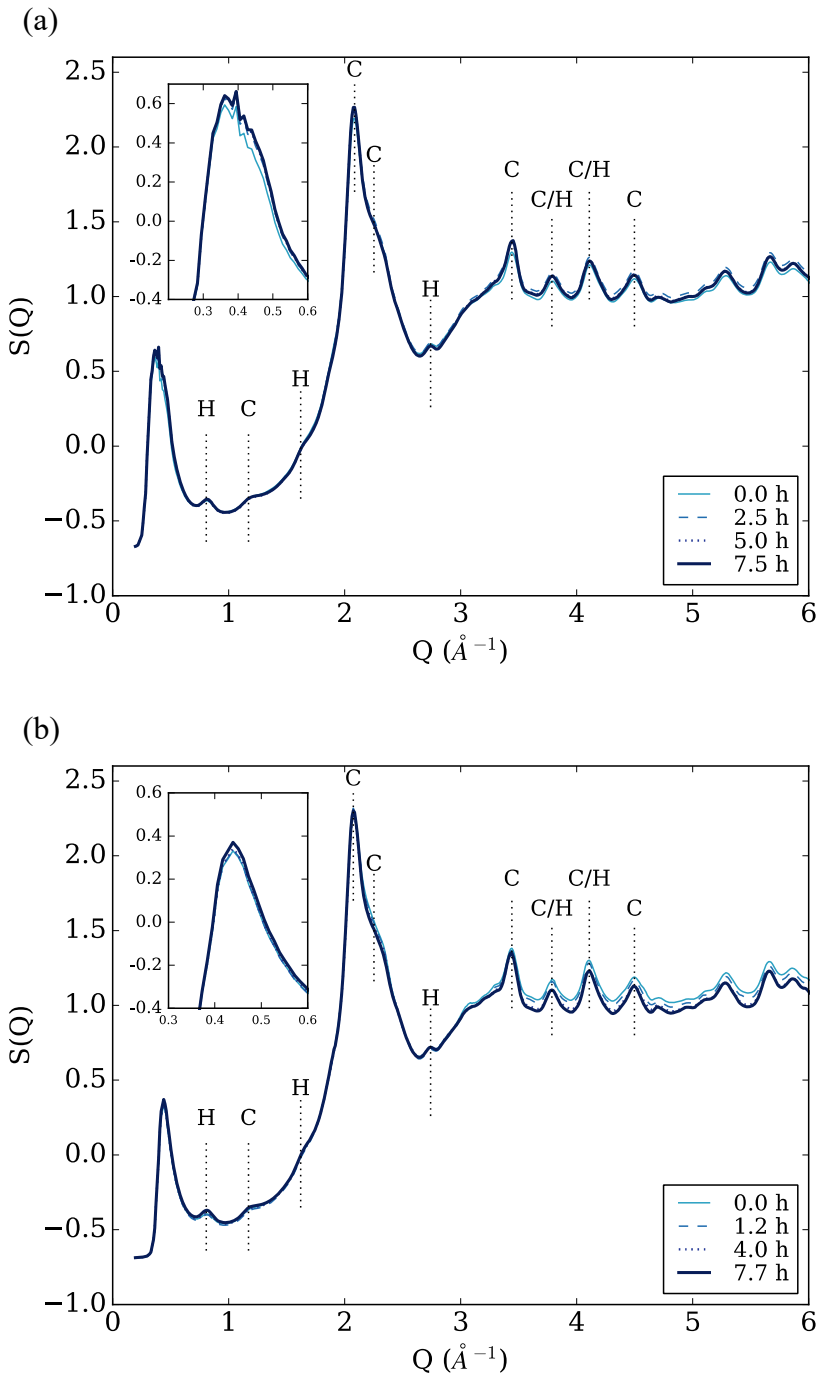

Figure S5. X-ray diffraction patterns of the silicate-activated slag sample (a) without and (b) with nano-ZrO_2 in 43% RH environment as a function of time. “C” denotes the C-(N)-A-S-H phase while “H” represents the hydrotalcite-like phase.

PDF of silicate-activated slag with nano-ZrO_2 over an *r* range of 10 to 22 Å

It is seen from Figure S6 that the *r*-spacing shift in the PDF data for silicate-activated slag with nano-ZrO_2 is less obvious for both the 0% and 43% RH condition compared to silicate-activated slag without nanoparticles (see Figure 4 in the article). For silicate-activated slag with nano-ZrO_2 in 0% RH environment (Figure S6a), the peaks at 13.3 and 15.6 Å shift in an opposite direction compared to those for silicate-activated slag without nanoparticles (Figure 4a in the article). The peaks at 11.1 and 16.9 Å show minimal change. On the other hand, most of the peaks of silicate-activated slag with nano-ZrO_2 in 43% RH environment show no change except for the one at 20.3 Å, which is likely associated with growth of the "unconventional" gel instead of a shoulder shift.

(a)

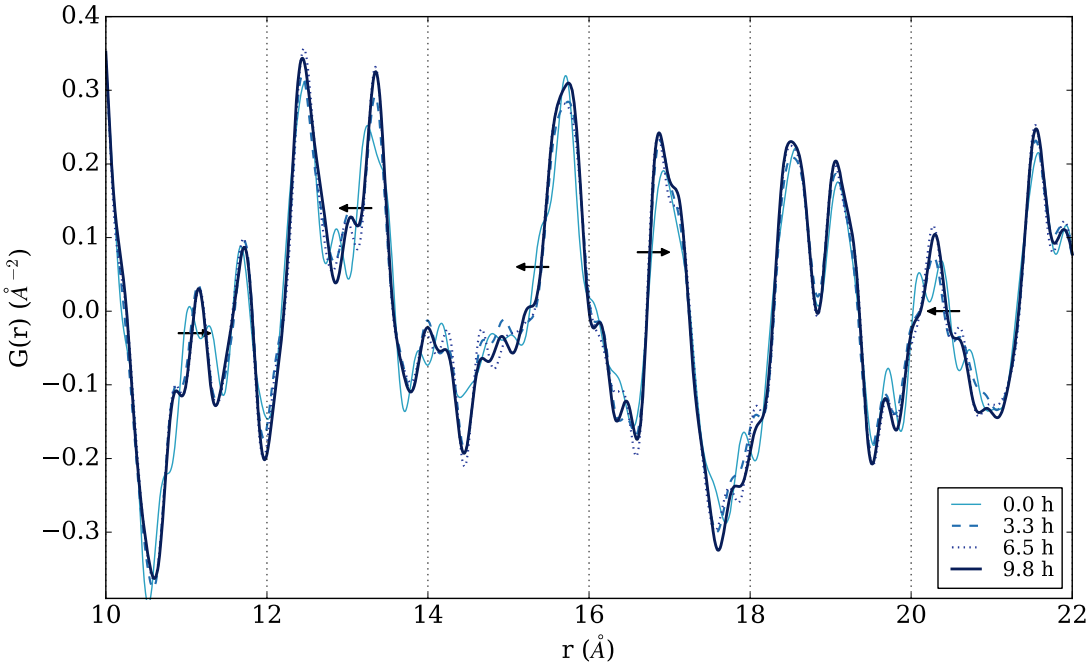

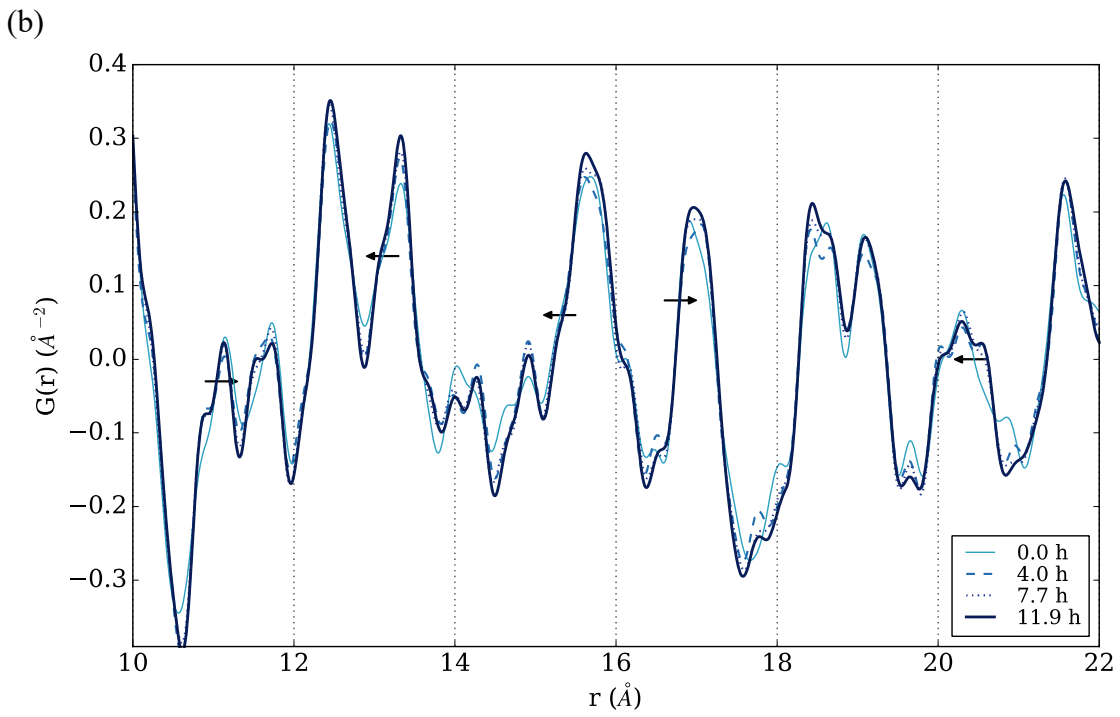

Figure S6. Synchrotron X-ray PDF curves of the silicate-activated slag with nano-ZrO_2 at (a) 0% RH and (b) 43% RH for different drying times, over an r range of $10 < r < 22$ Å. Black arrows indicate the direction of peak shift for silicate-activated slag without nanoparticles at 0% RH shown in Figure 4a of the article.

Effect of nano-ZrO_2 on the formation kinetics of silicate-activated slag

Given that nano-ZrO_2 is utilized here as a potential method to augment the drying-induced atomic structural changes, we first need to elucidate if the nanomaterial is affecting the alkali-activation reaction prior to analysis of the drying-related behavior. Comparison of the PDF data of the control silicate-activated slag samples with and without nanoparticles (Figure S1) reveals that nano-ZrO_2 has little impact on the evolution of the atomic structure and the kinetics of the alkali-activation reaction. It has been previously shown that the emergence of the Ca-T peak in alkali-activated slag during formation is a direct measure of the amount of C-(N)-A-S-H gel in the sample.[5] Figure S7

shows the evolution of this peak for silicate-activated slag with and without nanoparticles, where it is clear that the C-(N)-A-S-H gel precipitates at approximately the same rate in both systems. However, between 30 and 50 hrs, the sample with nanoparticles is seen to have a slightly higher rate of gel growth followed by a suppressed growth region from 50 to 90 hrs. These results imply that nano-ZrO_2 may slightly accelerate C-(N)-A-S-H gel formation in silicate-activated slag during the first few days of alkali-activation, but the atomic structure and amount of C-(N)-A-S-H gel that is present in the sample after several months is found to be the same, irrespective of the amount of nano-ZrO_2 used (unpublished work, up to 1% wt. nano-ZrO_2 has been analyzed). Similar behavior is seen in the isothermal conduction calorimetry (ICC) data for silicate-activated slag with and without nano-ZrO_2 (Figure S8). Among the limited literature on the influence of nano-ZrO_2 on the kinetics of OPC formation, Nazari and Riahi reported mixed results when the cement paste was cured in water, but a consistent trend was seen for samples cured in lime water, where acceleration of the reaction was noted for higher amounts of zirconia nanoparticles.[9] Therefore, analysis of the PDF data reveals that nano-ZrO_2 does not significantly influence the type of C-(N)-A-S-H gel that forms during the alkali-activation reaction, nor does it substantially alter how quickly the gel forms during the activation process.

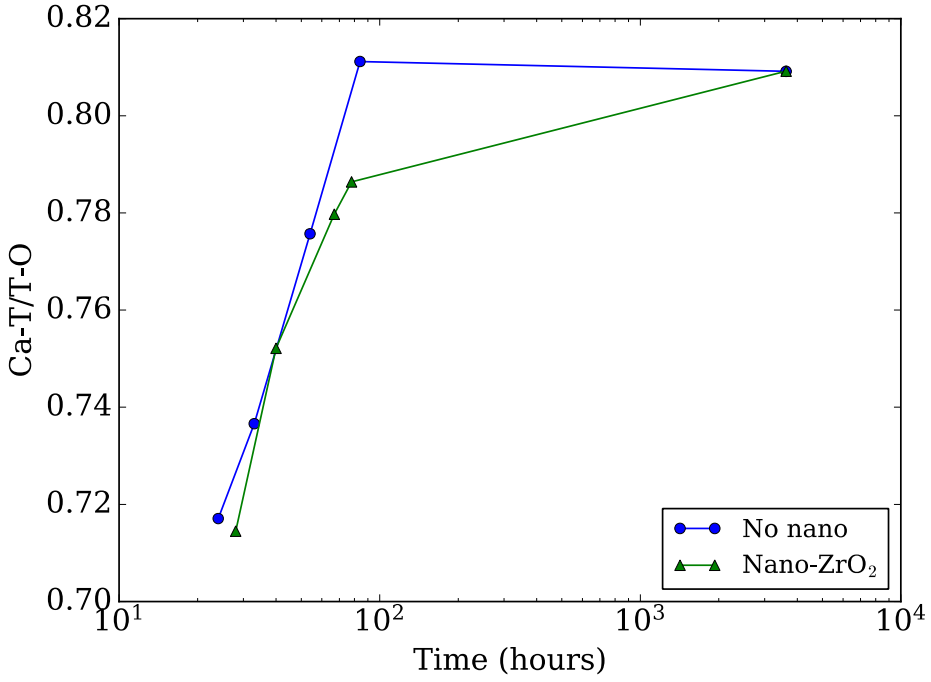

Figure S7. Evolution of normalized Ca-T (T is Si or Al) peak intensity of control silicate-activated slag with and without nano-ZrO_2. The time axis is given on a logarithmic scale.

Isothermal conduction calorimetry data of silicate-activated slag with and without nano-ZrO_2

ICC was conducted on silicate-activated slag using a TAM Air (TA Instruments) in order to probe the impact of nano-ZrO_2 on the kinetics of the alkali-activation reaction. Five grams of each paste was tested using plastic containers at 25 °C. The data were collected for 100 h after mixing. The initial 1 hr of data were disregarded due to two reasons: (1) samples were synthesized outside the calorimeter, so 30–40 minutes were lost due to preparing and transferring the samples, (2) the calorimeter was found to be sensitive to the disturbances caused by insertion of the samples, so the initial 20–30 minutes after sample insertion were used to stabilize the instrument.

It is seen from Figure S8 that the evolution of heat flow for the silicate-activated slag with three different concentrations of nano-ZrO_2 are largely identical. The inset in Figure S8, which shows the major peak of heat release at ~ 12 hrs, indicates a subtle difference between the three cases where the peak for silicate-activated slag with 0.1% nano-ZrO_2 occurs earlier than the two other samples.

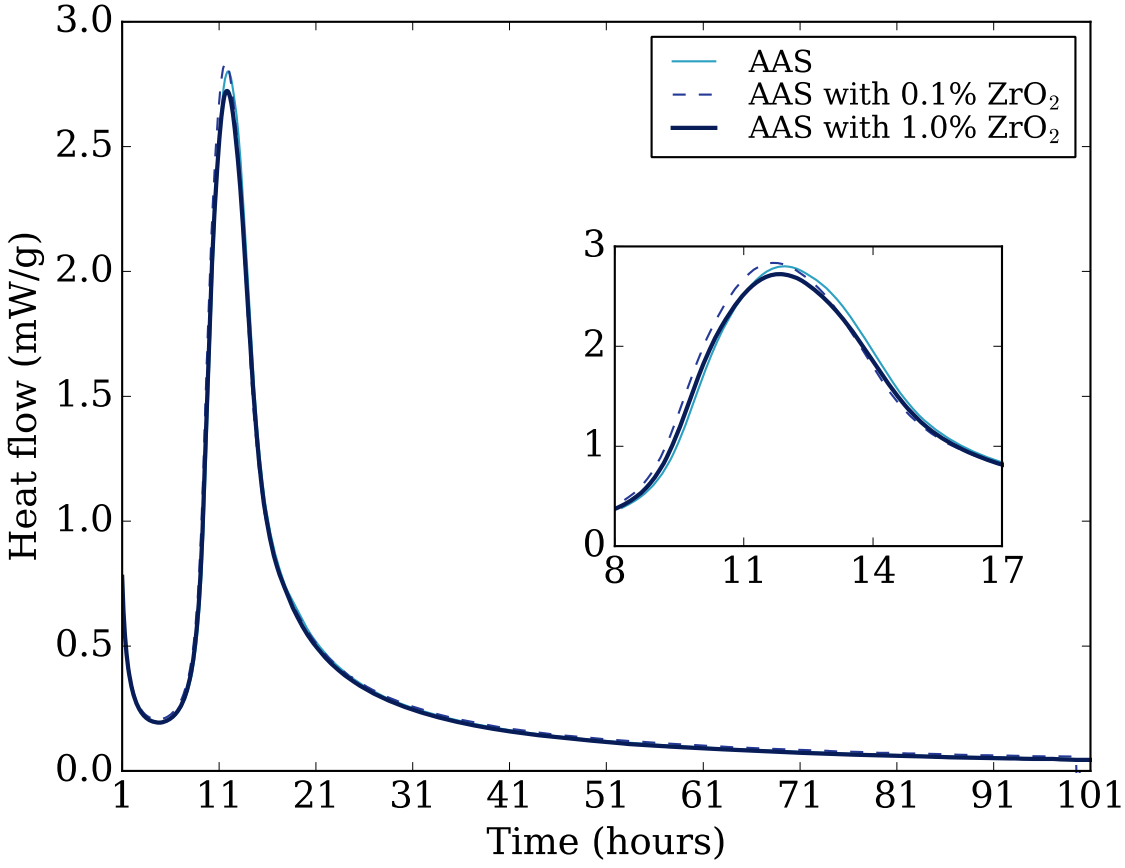

Figure S8. ICC data of silicate-activated slag (denoted as "AAS" in figure) with different amounts of nano-ZrO_2. The inset shows the zoomed-in major peak at ~ 12 hrs.

Examination of the appearance of nano-ZrO_2 in the PDF data of silicate-activated slag

In order to check if scattering from the zirconium atoms in nano-ZrO_2 in silicate-activated slag contributes to the PDF data, which might influence subsequent interpretation of the PDF data, the difference curve for the PDF data of silicate-activated slag with and without nanoparticles at the start of the drying experiment (0 hr) is plotted and compared with PDF data of the nano-ZrO_2 solution (Figure S9). Since the intensity of the difference plot is low, it has been scaled so that its first peak (a termination ripple) at ~ 0.5 Å aligns with that of the ZrO_2. A peak at ~ 2.1 Å in the difference curve overlaps with that of the nano-ZrO_2, which represents the correlation between zirconium and oxygen atom, but this peak in the difference curve is likely attributed to termination effects as opposed to nano-ZrO_2. Apart from this peak, no other overlapping peaks can be found. There is a strong peak at ~ 3.6 Å in the PDF data of ZrO_2, representing the distance between the two nearest zirconium atoms. In contrast, no distinct atom-aotm correlation is found at that location in the difference plot. This shows that the ZrO_2 in the silicate-activated slag does not contribute to the PDF data presented in the main article.

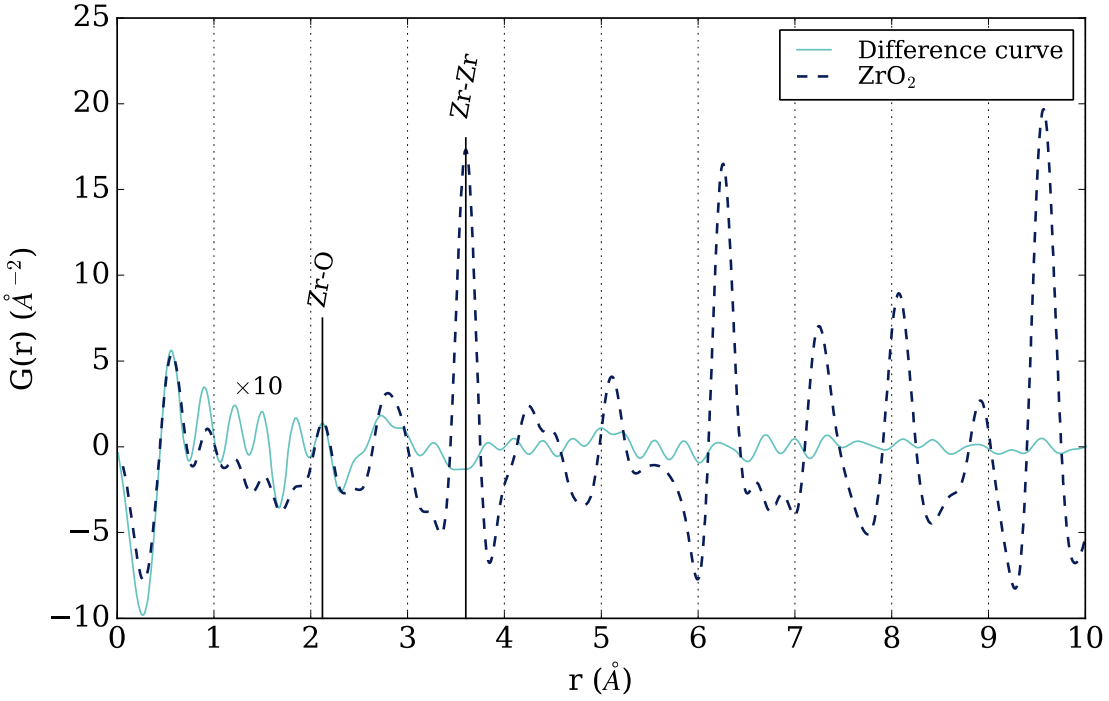

Figure S9. Difference PDF curve of silicate-activated slag with and without nano-ZrO_2 at 0 hr (i.e., immediately prior to commencement of drying), and the PDF curve of nano-ZrO_2 solution. The difference curve has been scaled (x10) such that the intensity of the first feature at ~ 0.5 Å matches the nano-ZrO_2.

Weight loss experiment

A weight loss experiment was carried out to examine if the rate of water evaporation is similar for silicate-activated slag with and without nano-ZrO_2 at 0% RH. Samples were prepared using the same method outlined in the Materials and Methods section in the article. Each powdered sample was placed in a glovebox purged constantly with dry nitrogen, and the weight was monitored using a balance (Mettler Toledo ML204T, precision: 0.1 mg) until equilibrium was reached. The weight of the silicate-activated slag with and without nano-ZrO_2 prior to drying was 3.31 and 4.55 g, respectively.

Figure S10 shows that the evolution of the weight loss is similar for silicate-activated slag with and without nanoparticles. Given a water/slag ratio of 0.44, it is calculated that ~ 63% of the water has evaporated from both samples at the end of the weight loss experiment. The final amount of weight loss is about 13% for both silicate-activated slag with or without nano-ZrO_2, which is about $\frac{13}{100-13} = 15\%$ with respect to the dried mass.

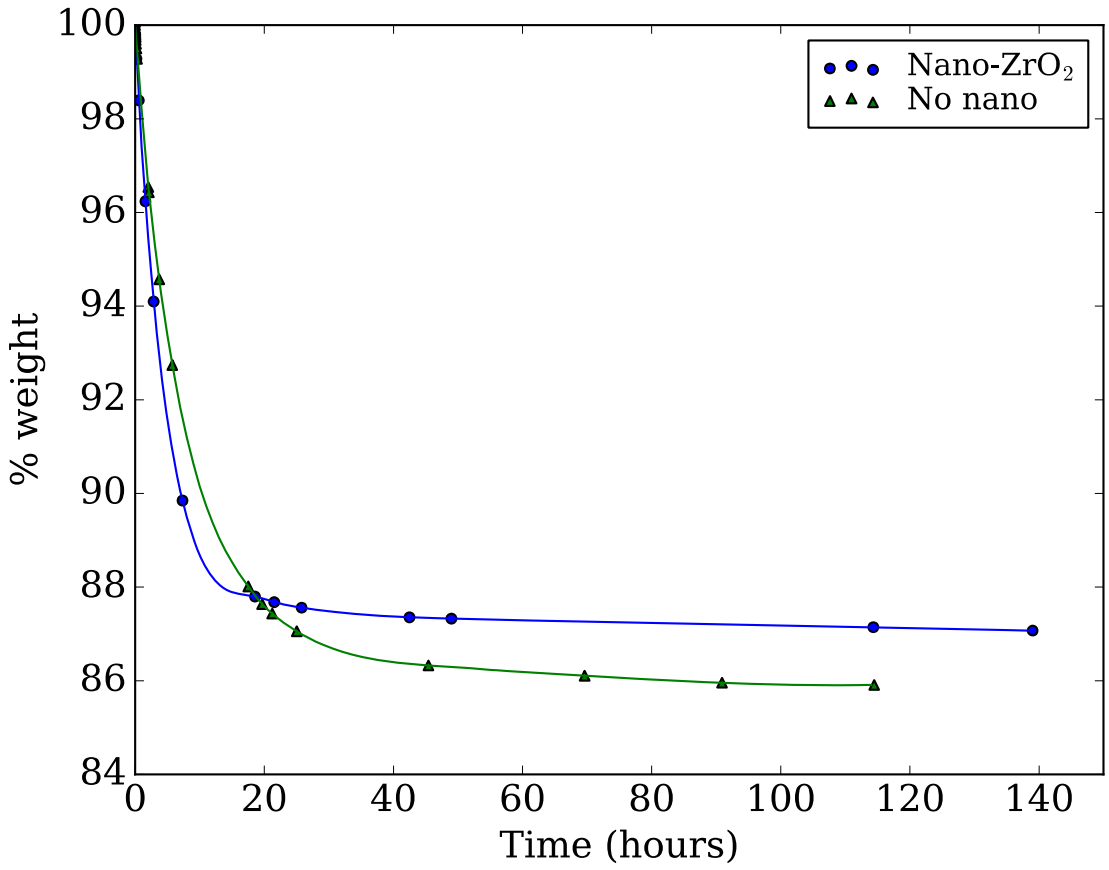

Figure S10. Evolution of the weight percentage of silicate-activated slag with and without nano-ZrO_2 in a 0% RH environment.

Stability of nano-ZrO_2 in silicate-activated slag during alkali-activation

The stability of nano-ZrO_2 in the silicate-activated slag has been investigated to elucidate if the zirconia surfaces (and internal structure) associated with the nanoparticles are still present in the sample during drying. This has been carried out by comparing PDF data at different times during the alkali-activation reaction (up to 131 days) with the PDF of nano-ZrO_2 in solution (i.e., stable nanoparticle suspension). Difference curves from the PDF data were obtained by subtracting the PDF curve of silicate-activated slag without nano-ZrO_2 from the sample with nanoparticles at different activation times, and therefore the difference curves show the additional phase(s) present in the nanoparticle doped system (Figure S11). It should be noted that the amount of nano-ZrO_2 in the silicate-activated slag used to generate Figure S11 is 1.0 wt. %, which is higher than the dosage used in the drying experiment (0.167 wt. %). This accounts for the reason why the low amount of nanoparticles cannot be detected in the PDF data in Figure S9, whereas they can be detected here given a higher amount.

As can be seen clearly in Figure S11, the difference curves, at all ages, reveal the presence of nano-ZrO_2 in the silicate-activated slag containing nanoparticles. This stable presence suggests that nano-ZrO_2 undergoes little to no dissolution during the alkali-activation reaction. In contrast, some nanoparticles, specifically ZnO nanoparticles have been recently found to dissolve during the alkali-activation reaction.[5] Thus, a stable presence of nano-ZrO_2 implies that their high surface area is available throughout the alkali-activation reaction in a sealed or drying environment.

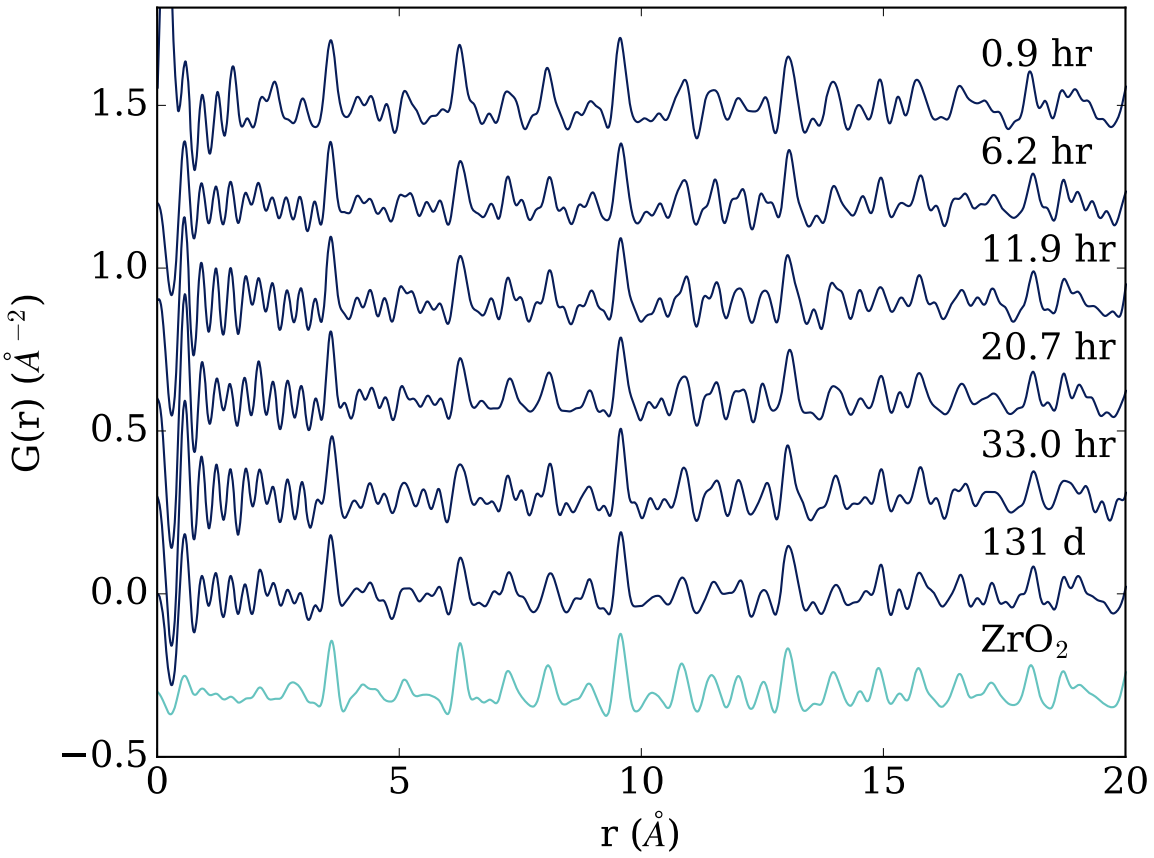

Figure S11. Stacked plot of the PDF difference curves during alkali-activation obtained by subtracting the X-ray PDF curve of the silicate-activated slag sample without nanoparticles from the PDF curve of the sample doped with 1.0 wt. % nano-ZrO_2 at the corresponding time. The experimental PDF of the nano-ZrO_2 solution is also plotted for comparison.

Size distribution of the ZrO_2 nanoparticles

The size distribution of the ZrO_2 nanoparticles has been determined using dynamic light scattering (DLS). Using a Zetasizer Nano-ZS (Malvern Instruments, Southboro, MA), the nanoparticle diameter and polydispersity index (PDI) were determined at 25 °C with a detection angle of 173°. Three measurements were carried out to assess reproducibility of the results. DLS data were

processed with Malvern's software using a distribution analysis based on a cumulant model. The cumulant analysis is defined in the International Organization for Standardization (ISO) standard document 13321. The calculations of PDI are defined in the ISO standard document 13321:1996 E.

Figure S12 shows the size distribution of the ZrO_2 nanoparticles used in this study. It is seen that the distribution is unimodal, with size ranging from 40 – 300 nm. The average particle size is 127.7 ± 2 nm, where the standard deviation was obtained from repeating the measurement for three times. The PDI is 0.143 ± 0.003 (0.146, 0.140. 0.144), indicating a narrow size distribution.

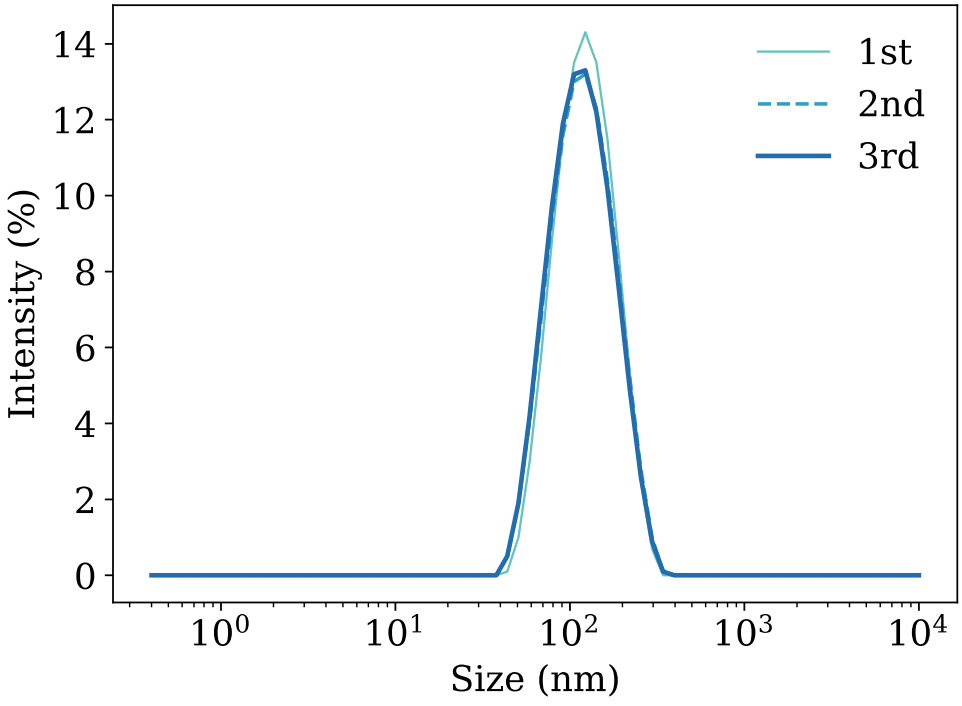

Figure S12. Size distribution of the ZrO_2 nanoparticles obtained using dynamic light scattering. The measurement was repeated three times to assess reproducibility of the results. Size is given on a logarithmic axis.

References

1 C. Meral, C. J. Benmore and P. J. M. Monteiro, *Cem. Concr. Res.*, 2011, **41**, 696–710.

2 L. B. Skinner, S. R. Chae, C. J. Benmore, H. R. Wenk and P. J. M. Monteiro, *Phys. Rev. Lett.*, 2010, **104**, 195502.

3 K. Gong and C. E. White, *Cem. Concr. Res.*, 2016, **89**, 310–319.

4 C. E. White, J. L. Provis, B. Bloomer, N. J. Henson and K. Page, *Phys. Chem. Chem. Phys.*, 2013, **15**, 8573–8582.

5 N. Garg and C. E. White, *J. Mater. Chem. A*, 2017, **5**, 11794–11804.

6 M. B. Pinson, E. Masoero, P. A. Bonnaud, H. Manzano, Q. Ji, S. Yip, J. J. Thomas, M. Z. Bazant, K. J. Van Vliet and H. M. Jennings, *Phys. Rev. Appl.*, 2015, **3**, 064009.

7 A. H. Narten, W. E. Thiessen and L. Blum, *Science*, 1982, **217**, 1033–1034.

8 L. B. Skinner, C. Huang, D. Schlesinger, L. G. M. Pettersson, A. Nilsson and C. J. Benmore, *J. Chem. Phys.*, 2013, **138**, 074506.

9 A. Nazari and S. Riahi, *Mater. Res.*, 2010, **13**, 551–556.